Noise Effects on Two Excitable Systems: Semiconductor Laser and Neuron Network Oscillations

Athena Pan, Wei-Mien Mendy Hsu
Department of Physics, University of California, San Diego

I. Introduction

An excitable system consists of three general states: rest state, excited (or firing) state, and a refractory (or recovery) state. When unperturbed, the system stays at its rest state. Under small perturbation, the system performs small-amplitude linear oscillations around its rest state. However, for large enough perturbation, the system can be driven out of its rest state and goes through the excited and recovery states before returning to its rest state [Linder]. Such response is highly nonlinear. There exists many excitable systems in nature. In this paper, we study two specific systems in detail: semiconductor laser with optical feedback and neuron network oscillation. We describe the theories used to model these two excitable systems and explain how noise can be introduced to induce coherence resonance in these systems.

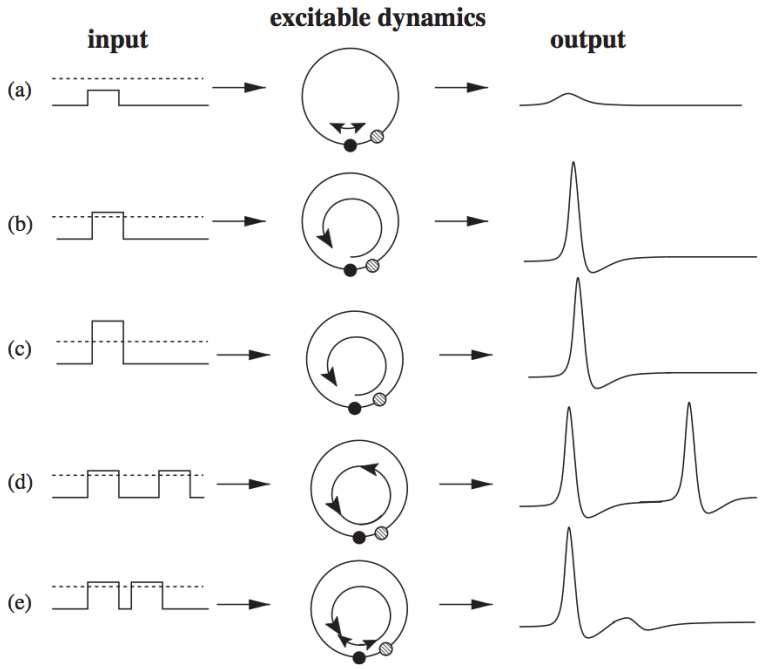

II. Correlated Noise Induced Optical Coherence Resonance

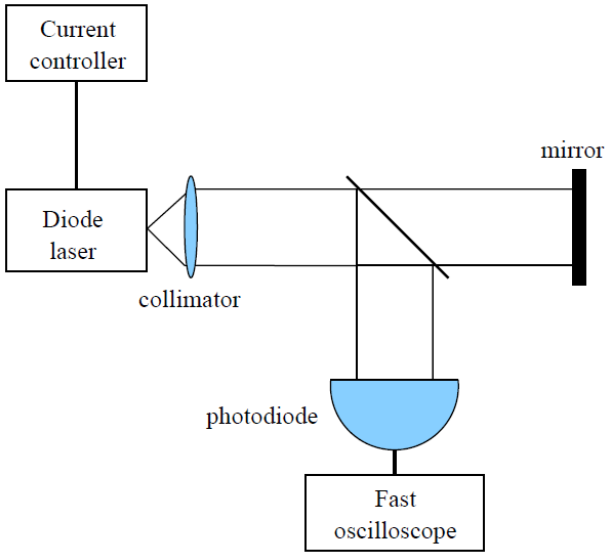

Fig. A. Experimental setup of a semiconductor laser with optical feedback [Lindner].

Semiconductor laser subjected to external optical feedback (Fig. A) can exhibit dynamical instability [10, 8]. Specifically, when the injection current is kept above, but close to, the solitary laser threshold, irregular dropouts in laser intensity can be observed [5]. Giacomelli et al has further shown experimentally that the coherence (or regularity) in the laser intensity dropouts can be tuned by changing the amount of input noise in the pump current. Coherence resonance can be observed for an optimal amount of noise, which is neither too large nor too small Fig. B [5].

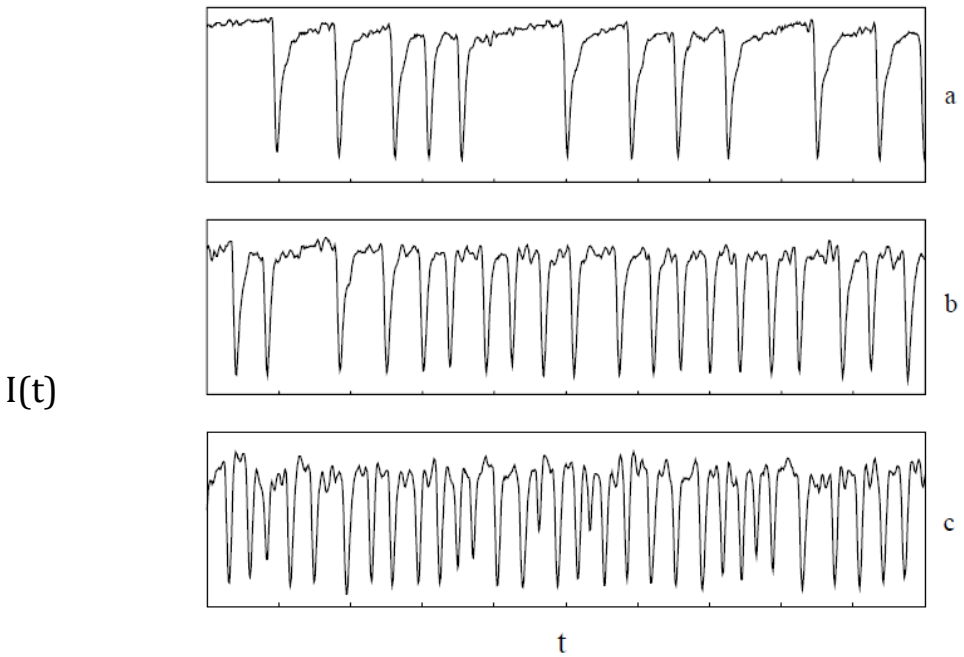

Fig. B. Temporal evolution of the intensity of a semiconductor laser with optical feedback. The noise level is (a) -60.8 dBm/MHz, (b) -52.5 dBm/MHz, (c) -44.3 dBm/MHz [5].

1. Lang-Kobayashi Model

The dynamics of semiconductor laser with optical feedback can be modeled with the Lang-Kobayashi (LK) model [7]. The LK model assumes the semiconductor laser is under single-mode operation and that multiple reflections from the external feedback mirror can be ignored due to low reflectivity. Under single-mode, single reflection conditions, we need only to add an extra term to the standard semiconductor laser rate equations to account for the feedback field [7, 4, 9]:

$$\frac{dE(t)}{dt} = \frac{1+i\alpha}{2}\left[G(E,N)-\gamma\right]E(t) + \kappa \times \exp[-i\omega\tau_f]E(t-\tau_f) + F_E(t), \quad (1)$$

$$\frac{dN}{dt} = \gamma_e\{CN_{th} - N(t)\} - G(E,N)\left|E(t)\right|^2. \quad (2)$$

The material-gain function can be expressed as follow:

$$G = \frac{g \times (N(t) - N_0)}{1 + s\left|E(t)\right|^2}. \quad (3)$$

The definition of all variables used above is summarized in table 1. The random fluctuation due to spontaneous emission is represented by $F_E(t)$, which is Guassian white noise with zero mean and δ correlated in time (i.e. $\left\langle F_E(t)F_E^*(t')\right\rangle = R\delta(t-t')$). The steady state solutions of the LK equations are of the following form [8, 10]:

$$E(t) = \sqrt{P_s}\exp(-i\Delta\omega_s t), \quad N(t) = N_{th} + n_s, \quad (4)$$

where $P_s = \left|E(t)\right|^2$, n_s is the carrier density change, and $\Delta\omega_s$ represent the frequency shift from the solitary laser frequency ω. Substituting equation (4) into (1), separating the real and imaginary part, we obtain the following two equations:

$$\Delta G = G(E,N) - \gamma = -2\kappa\cos(\Delta\omega_s\tau_f), \quad (5)$$

$$\Delta\omega_s = -\frac{\alpha}{2}\left[G(E,N)-\gamma\right] + \kappa\sin(\Delta\omega_s\tau_f) = \kappa(\alpha\cos(\Delta\omega_s\tau_f) + \sin(\Delta\omega_s\tau_f)). \quad (6)$$

Variables	**Definition**
$E(t)$	Complex electric field envelope inside the laser
$N(t)$	Excess carrier number
α	Linewidth enhancement factor
ω	Solitary laser frequency
γ, γ_e	Inverse of photon and carrier lifetime, respectively
κ	Feedback strength / rate, related to facet and external reflectivity [8]
τ_f	Time it takes for light to travel to the external mirror and back
$F_E(t)$	Langevin force → Gaussian white noise due to spontaneous emission
C	Pump rate, directly related to pump current
$N_{th} = \frac{\gamma}{g} + N_0$	Threshold carrier number

Table 1. Definition of variables in rate equations.

Combining equation (3), (4), (5), and (6), we see that $\Delta\omega_s$ and n_s are related by an elliptical equation [8]:

$$\left(\frac{gn_s}{2\kappa}\right)^2+\left(\frac{\Delta\omega_s}{\kappa}-\frac{\alpha gn_s}{2\kappa}\right)^2=1. \qquad (6)$$

That is the multiple solutions to the LK equations lie on an ellipse in the $(\Delta\omega_s, n_s)$ phase space. Fig. C shows a possible set of solutions in phase space. The characteristics equations of the Jacobian matrix of the LK equations are rather complicated [11]. However, it can be shown that solutions on the upper half of the ellipse, denoted by stars, are unstable saddle points, usually referred to as antimodes. The diamond in the center of the ellipse corresponds to the steady state solution in the absence of optical feedback. Solutions at the lower half of the ellipse, referred to as modes, may or may not be stable depending on many parameters — one of them being the feedback strength γ. The solution indicated by an arrow in Fig. C represents the maximum-gain mode (MGM). Operating under this mode, the laser is most efficient — outputting maximum power with minimum carrier density change n_s. Physically, it corresponds to optimal constructive interference between the intra-cavity field and the feedback field [8].

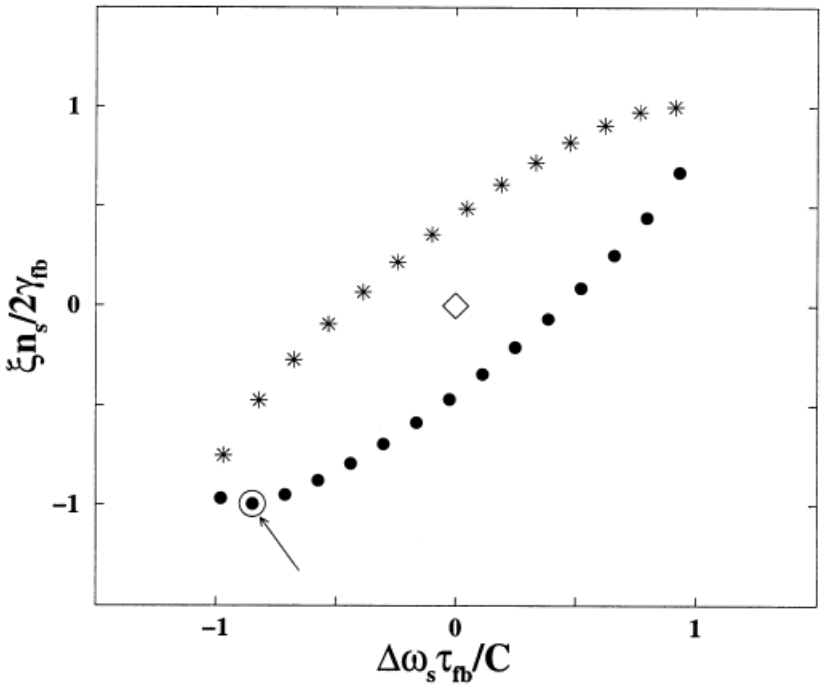

Fig. C. Steady state solutions (fixed points) of the LK equations in $(\Delta\omega_s, n_s)$ phase space [8].

For small feedback, the modes are stable and the laser operate at a frequency very close to its solitary frequency, ω. However, as the feedback strength increase, many of the modes also become unstable and the system attempts to move toward the MGM. However, before the system can reach the MGM, it passes by an antimode,

which "throws" the system back toward the center of the ellipse. Mulet *et al* numerically simulated the phase space trajectory for a semiconductor laser biased close to its threshold and subjected to optical feedback (Fig. D) [9]. As shown in Fig. D, as the system travels toward the MGM from other unstable modes (diamonds), it comes too close to an antimode (crosses), which drives the system toward the center of the ellipse, resulting in a dramatic increase in $\eta(t) = \phi(t) - \phi(t - \tau_f)$ and a intensity dropout. Here, $\eta(t)$ is the difference between the phase of the intra-cavity field $\phi(t)$ and that of the feedback field $\phi(t - \tau_f)$.

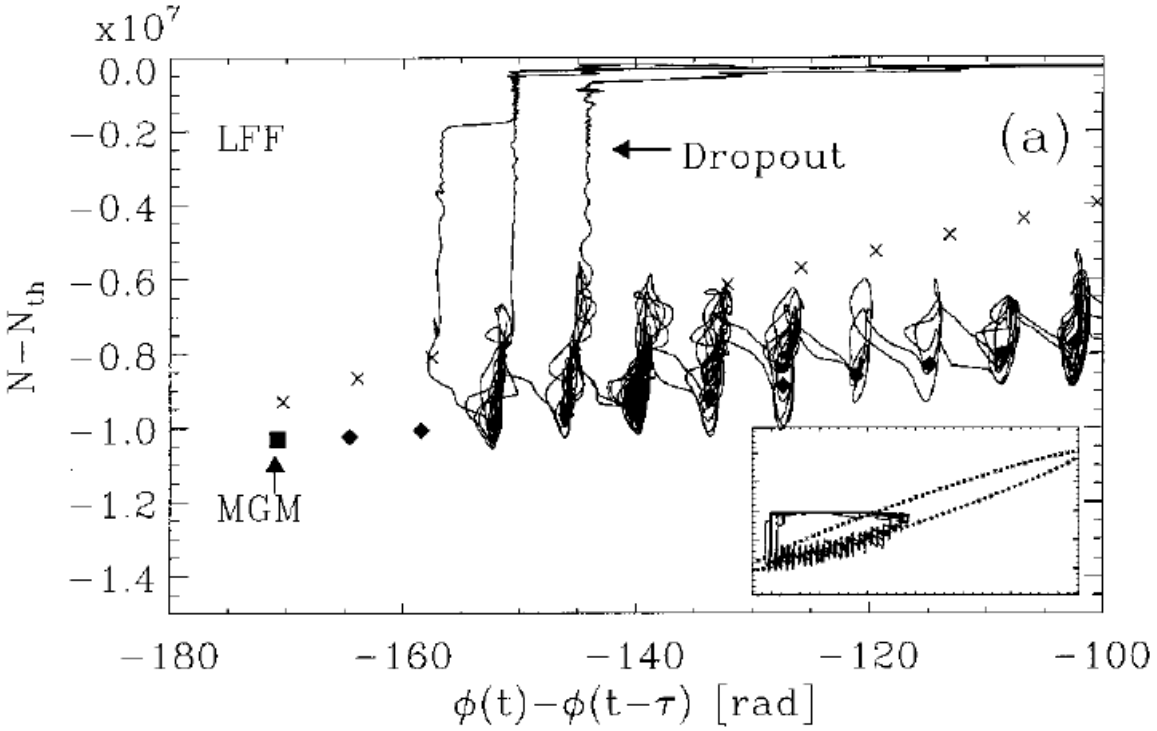

Fig. D. Evolution of the trajectory in phase space of a semiconductor laser with optical feedback and pumped close to threshold [9].

2. Optical Coherence Resonance

By tuning the noise characteristics in the pump current, Buldu *et al* showed that the coherence in the intensity dropouts can be optimized [4]. To model the pump current noise, an extra term, $\xi(t)$, was added to equation (2):

$$\frac{dN}{dt} = \gamma_e \{C[1 + \xi(t)]N_{th} - N(t)\} - G(E,N)|E(t)|^2. \qquad (7)$$

The system evolves in time scales on the order of tens of picoseconds, which is faster or of the order of the characteristic time scale of the fastest electrical modulation that can be introduced experimentally [6]. Therefore, the pump current noise cannot be adequately modeled with Gaussian white noise. Instead, Buldu *et al* adapted

correlated noise of the Ornstein-Uhlenbeck type, which is Gaussianly distributed with zero mean and correlation of form:

$$\langle \xi(t)\xi(t') \rangle = \frac{D}{\tau_c} \exp\left(-\frac{t-t'}{\tau_c} \right), \qquad (8)$$

where τ_c is the correlation time of the noise. One can solve equation (1), (7) and (8) numerically and recover the intensity dropouts or phase jumps in the time series of the laser output (Fig. E) [4].

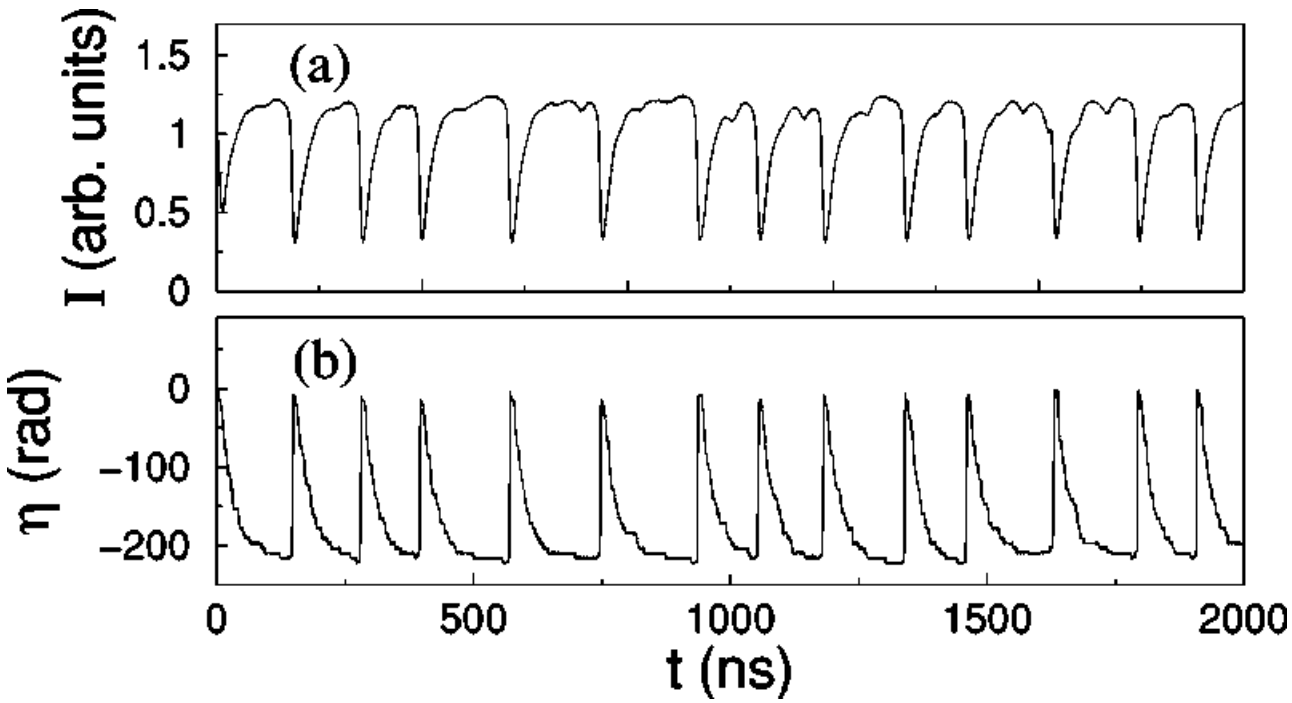

Fig. E. Simulated intensity and phase difference as a function of time. A peak in the phase difference between intra-cavity field and feedback field corresponds to a dropout in the intensity [4].

The noise level can be tuned in the simulation by changing the variance $\sigma = \sqrt{\frac{D}{\tau_c}}$. Fig. F shows the phase jumps as a function of time for three different values of σ. The phase jumps are most coherent (or regular) for moderate amount of noise $\sigma = 9.35 \times 10^{-2}$ (Fig. F(b)), which corresponds to perturbing the system in resonance. That is the average perturbation time interval is close to the system's intrinsic recovery time. For low noise level (Fig. F(a)), the perturbation is rarely large enough to drive the system out of its stable mode. Therefore, the time intervals between successive jumps in $\eta(t)$ are relatively large and less regular. For very high level noise (Fig. F(c)), the system is frequently driven out of its current mode before it has enough time to recover back to its stable mode. That is the average perturbation time interval is much shorter than the system's recovery time. Therefore, we see that the peaks in $\eta(t)$ broaden and the time intervals between successive peaks are irregular.

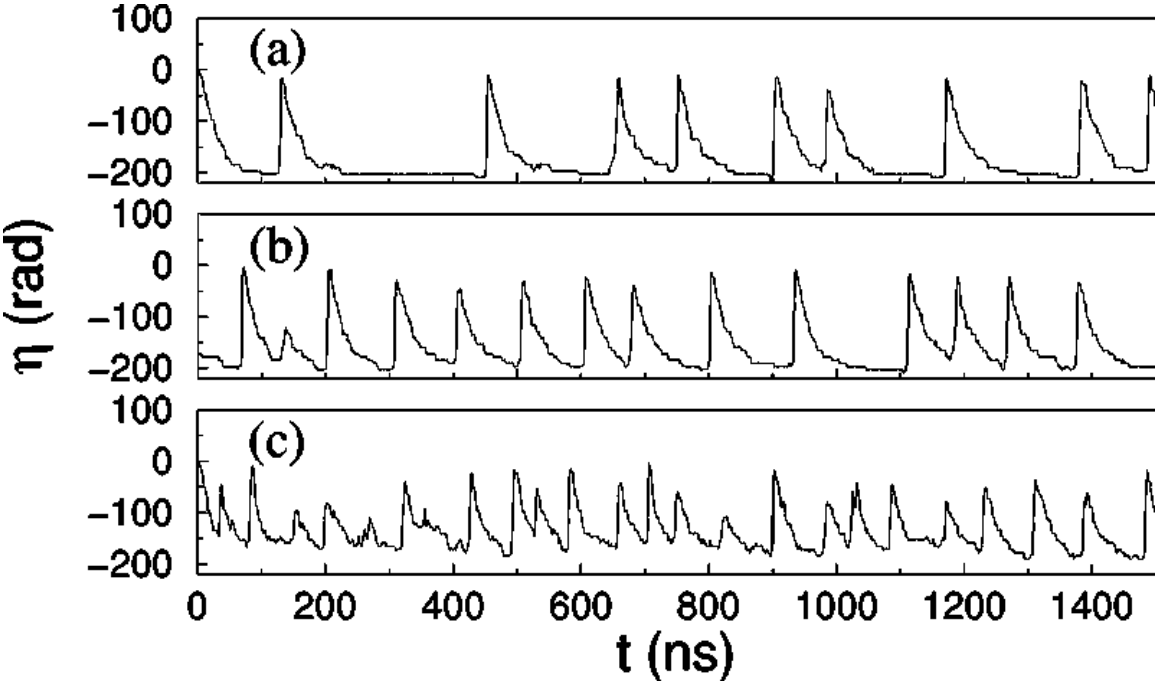

Fig. F. The coherence behavior of $\eta(t)$ as the noise level changes: (a) $\sigma = 7.36\times10^{-2}$, (b) $\sigma = 9.35\times10^{-2}$, (c) $\sigma = 1.60\times10^{-1}$. Noise correlation time is kept constant at $\tau_c = 24ps$ [4].

Interestingly, coherence resonance can also be observed by fixing the noise level $\sigma = \sqrt{\frac{D}{\tau_c}}$ and changing the noise correlation time τ_c. Fig. G(b) shows that the peaks in the phase $\eta(t)$ is most coherent for moderate correlation time $\tau_c = 57.6ps$ [4]. Short correlation time corresponds to high frequency modulation in the pump current. In this high frequency limit, the carriers dynamics in the semiconductor acts as a low-pass filter, preventing the system from responding to the high frequency modulation. Therefore, the intervals between successive peaks in Fig. G(a) are large and irregular. On the other hand, in the low frequency limit, or long correlation time, the carriers have enough time to respond and the system follows the noise modulation in the pump current. The incoherence in the noise naturally translates into the incoherence of the system output (Fig. G(c)). Only for moderate correlation time will the system responds in resonance.

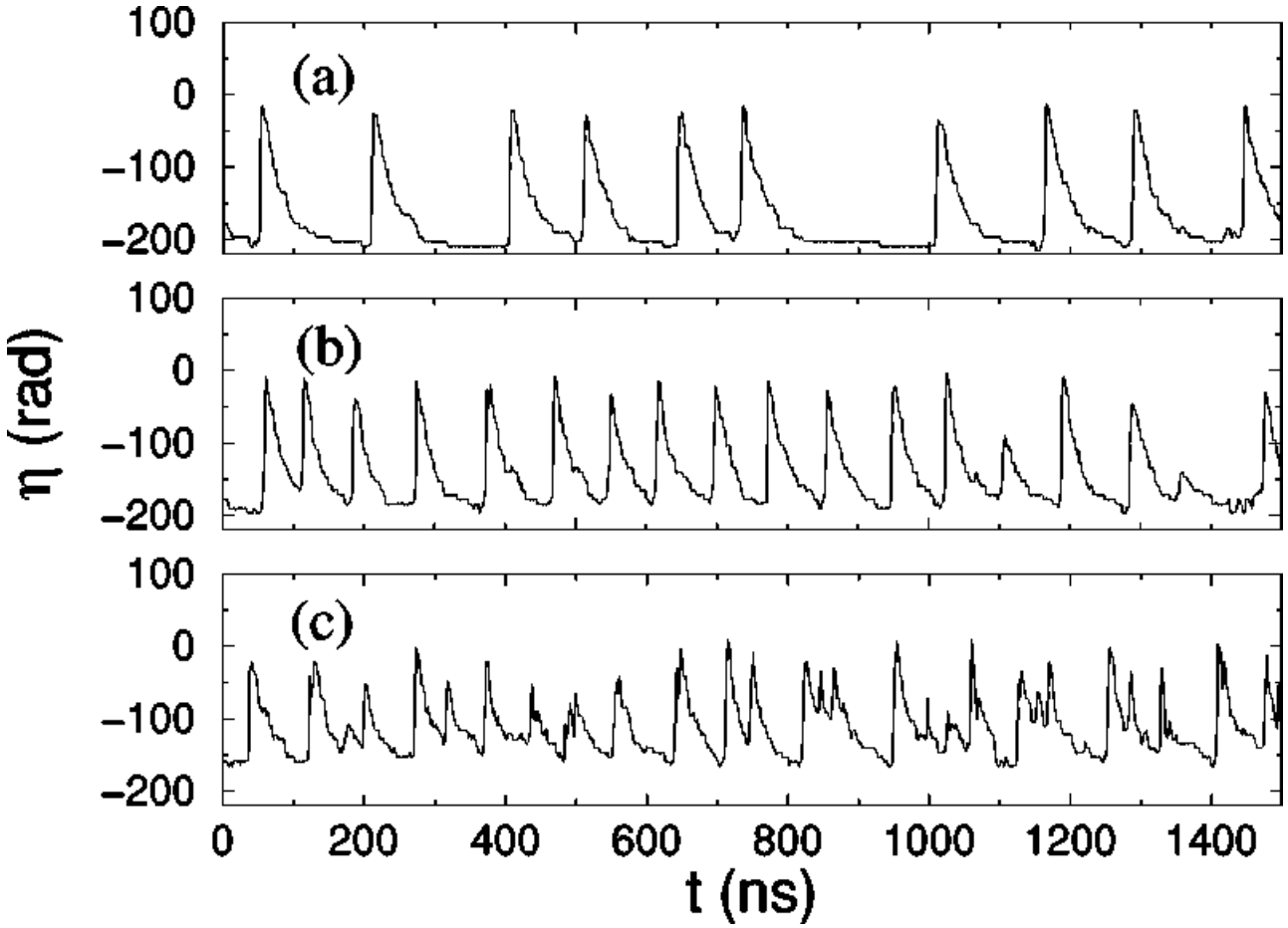

Fig. G. Coherence behaviors of phase difference $\eta(t)$ as the noise correlation time changes: (a) $\tau_c = 15.8ps$, (b) $\tau_c = 57.6ps$, (c) $\tau_c = 153.2ps$. Noise intensity is kept constant at $\sigma = 0.079$ [4].

III. Noise-Induced Network Oscillations in a Reduced Bursting Model

1. Resonant Integrate-and-fire Model

In this article, the author reduced the Hindmarsh-Rose (HR) model by modifying the integrate -and-fire (IF) model with a reset mechanism after a threshold crossing, as given by the two linear ODEs and the reset rules:

$$\frac{dx(t)}{dt} = Ax(t) + By(t) + I_{Signal}(t)\,, \qquad (1)$$

$$\frac{dy(t)}{dt} = Cx(t) + Dy(t)\,, \qquad for\ x(t) < x_{thres} \quad (2)$$

$$x(t) \to x_{reset}\,,\ y(t) \to y(t) + y_{reset}\,,\ \text{when } x(t) \text{ reaches } x_{thres}\,.$$

The $x(t)$ resembles a voltage-like variable while $y(t)$ describe the slow dynamic of an adapting current, similar to the slowly relaxing variable of HR model. The stationary state is at $(x, y) = (0, 0)$ while no input ($I_{Signal}(t)$) is applied. The first ODE behaves as integrate-and-fire model: when the voltage-like x reaches the threshold x_{thres}, $x(t)$ is reset to $x_{reset} < x_{thres}$ and meanwhile an action potential (spike) occurs, or more specifically saying, a sharp voltage change across the nerve membrane. To mimic the dynamic of HR model that a spike makes the increase of y, $y(t)$ will reset to $y(t) + y_{reset}$ whenever threshold crossing happens.

The four parameters A, B, C and D in RIF model are chosen to fit its impedance magnitude with that of HR model [S. Reinker, 2006], so as to mimic the subthreshold behavior of HR model—it exhibits a subthreshold resonance to signals with input periods near 336 time units [Reinker, 2003]. The fitting results given in the article are A= −0.032, B= −1.3258, C = 0.00025 and D= −0.001.

2. Results and Discussions

The Deterministic Firing in RIF Model

Deterministic cases with different sets of I_{Signal}, x_{reset}, y_{reset} and x_{thres} are shown in Figure 1. When $I_{Signal}(t) = 0$, the RIF system eventually evolves to equilibrium state $(x, y)_{I=0} = (0, 0)$. As constant $I_{Signal}(t) = 0.4$ applied, the system starts to cross threshold and fire regularly, and the firing frequency increases with the increase of the input intensity. Mathematically, with any constant input I_{Signal} the stable state is given as $(x, y)_I = I_{Signal}(-D, C)/\det(\gamma)$ [1]. However, with the threshold-crossing-and-firing mechanism in RIF model only when $-I_{Signal}/\det\gamma < x_{thres}$ will the system go to the stable state, otherwise it starts to firing periodically.

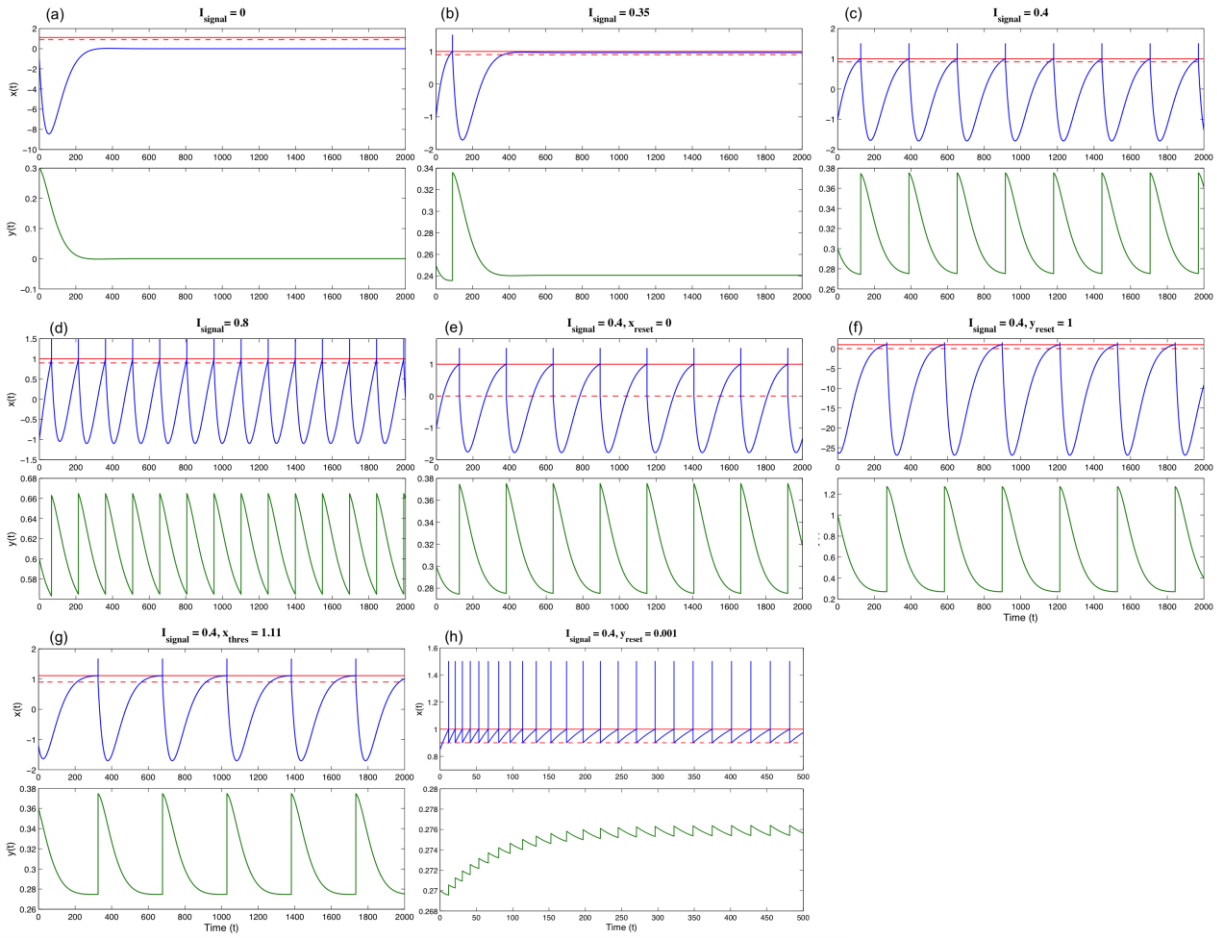

Fig. 1 The deterministic RIF model: (a) It goes to stable state when $I_{Signal}(t) = 0$. (b) As $I_{Signal} < -x_{thres}\det(\gamma)/D$, the system can not continuous the periodic firing. The presence of the first firing depends on the initial condition of (x_0, y_0) at $t = 0$. As long as x_0 is negative and y_0 is small enough, the dx/dt would likely to be positive that makes x reach the threshold in the early time steps. (c)-(g) shows the regular

[1] $\gamma = \gamma_{ij} = \begin{pmatrix} -A & -B \\ -C & -D \end{pmatrix}$, the same as defined in the Appendix.

firing patterns with different sets of I_{Signal}, x_{reset}, y_{reset} and x_{thres}. (c)&(d) The firing rate increases with I_{Signal} for that it is related with the increasing rate of x. (e) Lowering the x_{reset} to 0, the time course of inhibitory-to-firing is reduced such that the period of the firing pattern slightly decreases. On the other hand, the period will be prolonged if (f) y_{reset} is set to larger value 1 or (g) threshold is slightly lifted the to 1.11. (h) While y_{reset} is sufficiently small (0.01) that after each firing the dx/dt could still be positive, then it enters endless bursting phase.

The Stochastic Firing in RIF Model

Adding Gaussian white noise into RIF model, we get the two-dimensional stochastic differential equations which describes Ornstein-Uhlenbeck process

$$dx(t) = \left(-0.032x(t) - 1.3258y(t) + I_{Signal}(t)\right) dt + \sigma dW(t), \quad (3)$$

$$dy(t) = \left(0.00025x(t) - 0.001y(t)\right)dt\,, \qquad for\ x(t) < x_{thres} \quad (4)$$

$$x(t) \to x_{reset} = 0.9\,,\ y(t) \to y + y_{reset} = y + 0.1\,,\ \text{when } x(t) \text{ reaches } x_{thres} = 1,$$

where $W(t)$ denotes the Wiener process and the constant σ denotes noise intensity.

Figure 2 shows the stochastic FIR cases both with $I_{Signal}(t) = 0$ but different noise intensity σ. Interestingly, the noise not only can kick x to reach the threshold but also give rise to have multiple threshold crossings—the burst firings. Because after a firing the reset value of x is still close to the threshold, with sufficiently large noise it's highly possible to x to cross threshold again. However, each threshold crossing makes y increase by y_{reset}, and the larger the y is the more inhibition exerts on x. Therefore, bursting phase will be terminates at some time and entering the recover period.

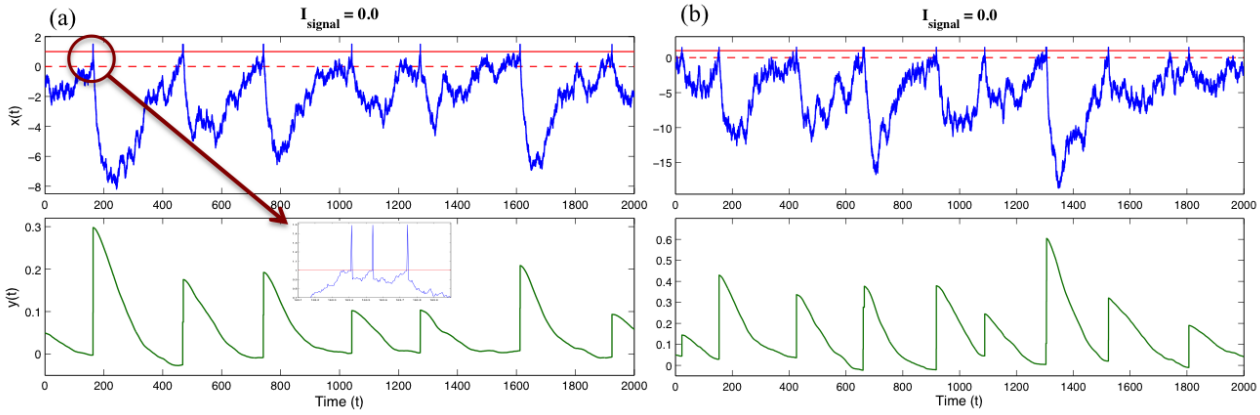

Fig. 2 The stochastic FIR with noise level (a) $\sigma = 0.2$ and (b) $\sigma = 0.5$, both demonstrate noise-induced multiple threshold crossings (bursts). The number of bursts in the same bursting phase can be tell form the increment of y value because we know each crossing make y increase by y_{rest}. In (a) around $t = 160$, y suddenly jumps to 0.3 indicating there are three times crossings, as shown in the inset. Note that as the noise level σ increases, not only the firing rate slightly increases but the number of bursts in the short time period distinctly increases as well.

Network behavior of RIF Model

To investigate the network properties of the RIF neurons, the simplest way is to bring an all-to-all coupling with an identical coupling strength Δ into the stochastic differential equations:

$$x_i(t + dt) = x_i(t) - \left(0.032x(t) + 1.3258y(t) - I_{Signal}(t)\right) dt + \sigma W(t) + \sum_{j \neq i}^{N} \Delta \delta_{x_j(t) \geq x_{thres}}$$

$$y_i(t + dt) = x_i(t) + \left(0.00025x(t) - 0.001y(t)\right)dt\,, \qquad for\ x(t) < x_{thres}$$

$x(t) \to x_{reset} = 0.9$, $y(t) \to y + y_{reset} = y + 0.1$, when $x(t)$ reaches $x_{thres} = 1$.

The summation in the first SDE models the synaptic coupling between N neurons by setting that the voltage of ith neuron will be lifted by the amount of Δ ($x_i \to x_i + \Delta$) whenever the jth neuron ($j \neq i$) fires. In other words, any one of the neuron j in the network crossing the threshold will make all the other neurons jump by Δ. Here we choose Δ to be positive so neurons are gradually pushed to threshold for each kick[2].

Figure 3 displays the raster plots of the coupled 50 RIF neurons with different sets of noise intensity σ and coupling strength Δ. Figure 3 (a)-(c) the coupling $\Delta = 0.06$ is fixed but with different noise intensity respectively. When noise level is low ($\Delta = 0.12$) the firing happens occasionally and is seemingly random. For intermediate noise ($\Delta = 0.02$) it demonstrates a synchronized and periodically firings among the network, but for sufficiently high noise ($\Delta = 0.9$) though the neurons still fire rapidly the synchronized activity disappears. Meanwhile, coupling strength Δ also has influence on this kind of stochastic oscillations, as shown in Figure 3 (d)-(f). With small noise intensity $\sigma = 0.08$, the network synchronization can only occur when the coupling strength is strong enough Figure 3 (e), and persist even with larger $\Delta = 0.2$ (f). The only difference between (e) and (f) is that its takes a while to start synchronize for a lower coupling strength.

[2] In a more complex neural network model, except for having the positive coupling, some portion of neurons will be set to have a negative Δ on the others so as to describe the inhibitory network behavior.

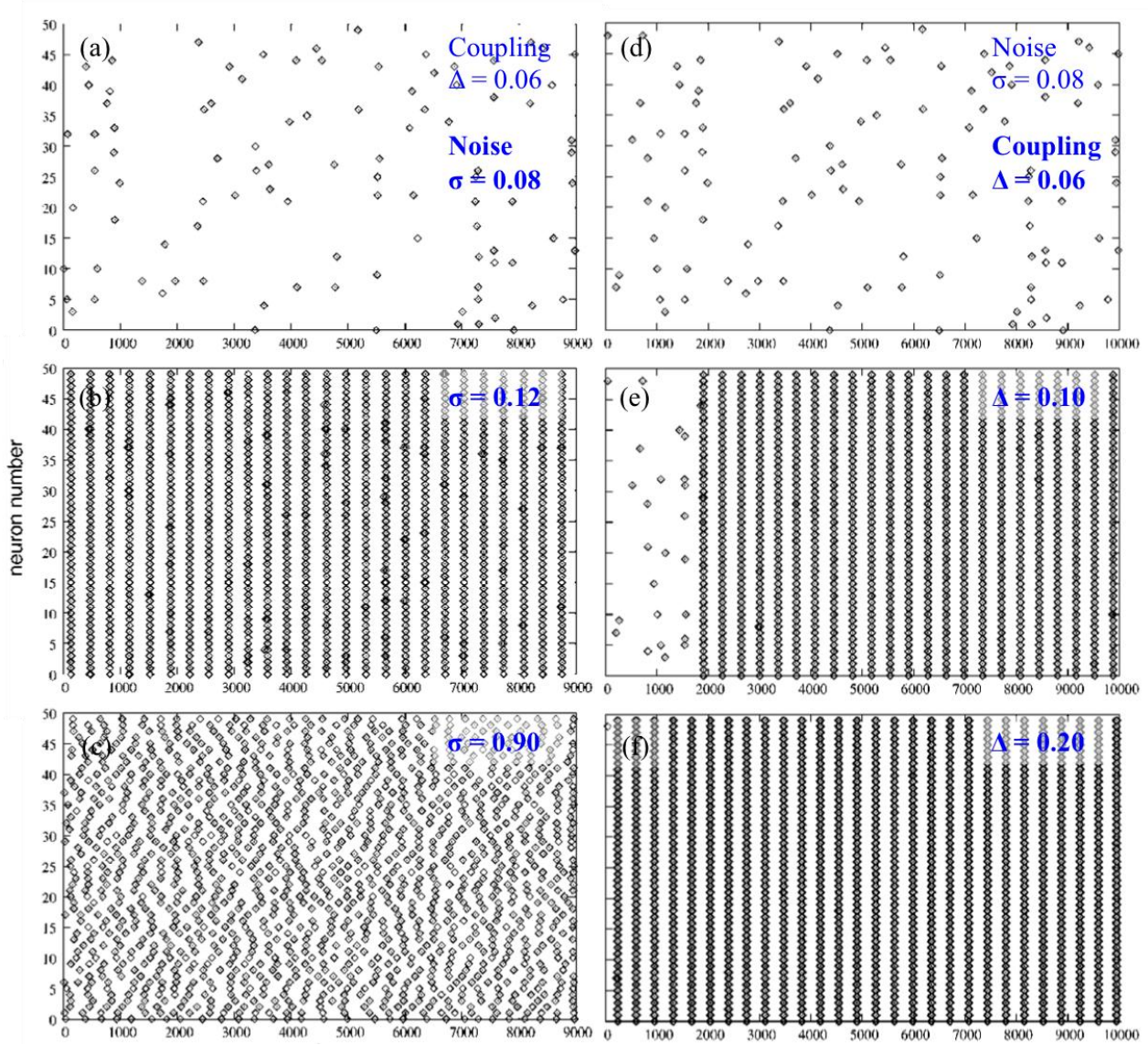

Fig. 3 (a)-(c) Raster plots of simulations of 50 RIF neurons [S. Reinker, 2006], with different noise level σ (a: 0.08, b:0.12, c:0.90) but with fixed coupling strength $\Delta = 0.06$. Synchronized stochastic network oscillations occur at intermediate noise strength and are stable over a wide range of σ values (between approximately 0.1 and 0.85). (d)-(f) The simulation with the dependence on coupling strength (d: 0.06, e:0.10, f:0.20) but fixed noise level $\sigma = 0.08$. The synchronized oscillations appear when the coupling is strong enough.

3. Stochastic Analysis of RIF Neural Network

During the bursts recovery period, the system is described by two linear stochastic differential equations Eq. (3) and (4), from which we can obtain its associated Fokker-Plank equation (FPE). By solving FPE we will get the probability distribution of the system that help us to clarify: 1) the system behavior during the burst recovery phase; 2) approximate the probabilities of threshold crossings, and 3) the expected number of neurons crossing threshold in the constrained system.

Following the procedure shown in Appendix, we got the unconstraint[3] probability density of one neuron, which is a Gaussian distribution

[3] The probability density can go over the threshold x. Even it's not

$$P(x,y,t) = \frac{1}{2\pi\sqrt{N_{11}N_{22} - N_{12}^2}} \exp\left\{ -\frac{1}{2\left(1 - \frac{N_{12}^2}{N_{11}N_{22}}\right)} \left(\frac{(x-M_1)^2}{N_{11}} - \frac{2N_{12}(x-M_1)(y-M_2)}{N_{11}N_{22}} + \frac{(y-M_2)^2}{N_{22}} \right) \right\},$$

where $M_1(t)$ and $M_2(t)$ are the center of the Gaussian (the first moments of x and y), $N_{11}(t)$ and $N_{12}(t)$ are the variances which is proportional to σ^2 (noise intensity), and $N_{12}^2/N_{11}N_{22}$ is the correlation coefficient. Since threshold only exists in x variable, it is convenient to consider the marginal probability density for x

$$P(x,t) = \int dy\, P(x,y,t) = \frac{1}{\sqrt{2\pi N_{11}}} \exp\left\{ -\frac{(x-M_1)^2}{2N_{11}} \right\}.$$

Also, the quantity $q(t)$ is define as the probability that $x > x_{thres}$ in the unconstrained and uncoupled system at time t,

$$q(t) = \int_{x_{thres}}^{\infty} P(x,t).$$

Figure 4 (a) and (b) show the time evolution of $P(x,t)$ for a single neuron with different noise level. As we see the $P(x,t)$ moves toward the stable point $x = 0$ and arrives there roughly at $t = 300$ to 350. From Appendix, we know the variance of $P(x,t)$, N_{11}, is proportional to σ^2. Therefore, as $P(x, t \geq 330)$ centered at $x = 0$, the fraction of $P(x,t)$ that lies outside of threshold x_{thres} is σ-dependent. The larger the σ is, the larger the portion of the tail of $P(x,t)$ falls in the range $x > x_{thres}$, shown in Figure 4 (c), and the higher the probability to have threshold crossing. And this threshold-crossing probability has been defined as $q(t)$ and shown in Figure (d).

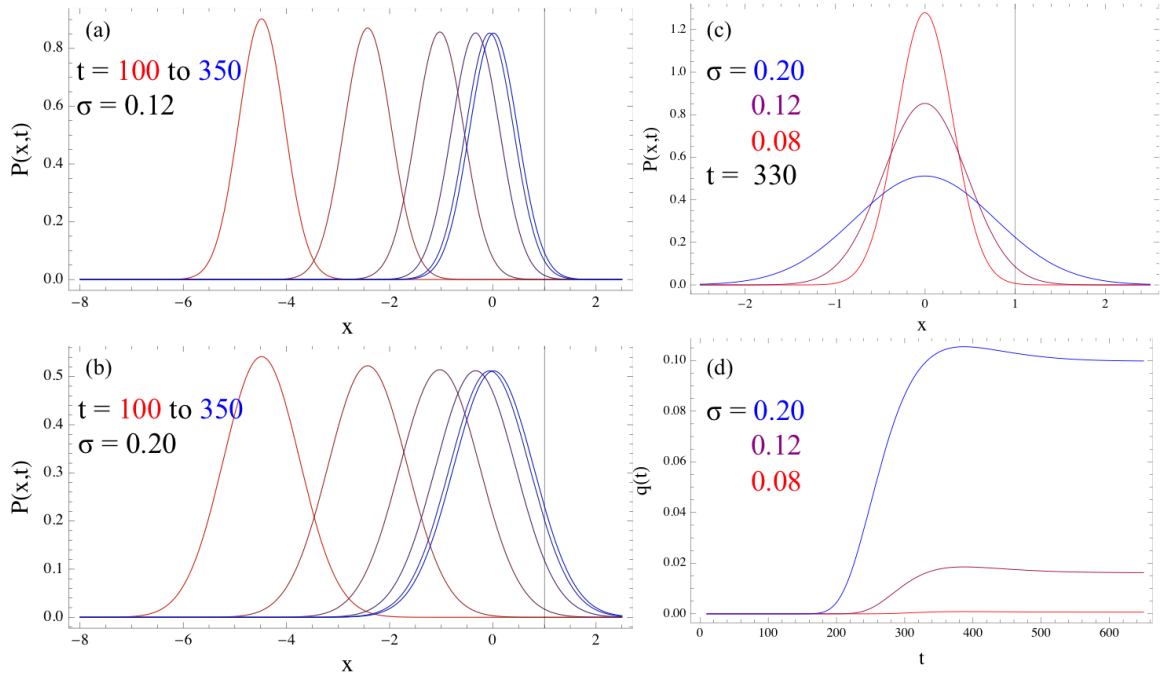

Fig. 4 (a) and (b) shows $P(x,t)$ at t=100, 150, 200, 250, 300, and 350 with the noise level σ =0.12 and 0.20, respectively. (c) $P(\mathrm{x}, \mathrm{t} = 330)$ with different noise intensity. The portion of the tail of the density P that exceeds x_{thres} is directly related to the variance of the distribution, which is proportional to the square of the noise intensity (σ^2). (d) the largest σ has the dramatically increases in $q(t \geq 200)$ while for small σ $q(t)$ is very close to 0, denoting that the high σ leads to the high probability of threshold crossing at the most likely time $t \approx 330$.

Another quantity $\mu(t, \Delta t)$, defined as the average number of neurons that cross the threshold x_{thres} spontaneously at a given time interval of length Δt, is given as

$$\mu(t, \Delta t) \approx N\bar{q}\Delta t$$

where $\bar{q}$ is the average of $q(t)$ over the period t to $t + \Delta t$. Form figure 4 (d) we know $q(t)$ reaches maximum at $t \geq 300$ and almost stays as a constant afterward. Therefore μ indicates how likely the isolated neurons are to cross threshold at time t. For different noise level, their μ values at $t = 325$ are shown in Table 1.

Table 1 The larger noise level has the larger μ, i.e., the threshold crossing is more likely to happen with higher noise.

$t = 325$, $\Delta t = 1$

σ	$\overline{q_j}$	μ
0.08	0.000005	0.00026
0.12	0.0016	0.08

With the quantities $q(t)$ and μ, we can explain how a small number of firing neurons can kick the system to bursting phase. The mechanism of coupling Δ, lifting the voltage by Δ whenever one neuron fires, is equivalent to shift the center of $P(x, t)$ to approach x_{thres} the by the amount of Δ, i.e., $P(x - \Delta, t)$. This shift in P makes its right tail enter the range $x > x_{thres}$, and increases $q(t)$, as shown in figure 5. For the case with slightly larger $\Delta = 0.10$ shown in figure 3 (e), the synchronization doesn't exit until time 2000. Obviously, with small Δ the majority of neurons may have to be pushed multiple times so as to shift their $P(x, t)$ sufficiently, which increases $q(t)$ to higher probability. Thus, in the beginning the firing pattern is seemly random due to just few of the neurons originally closed to threshold can cross the threshold. However, when these neurons fire the rests will also be pushed to approach the threshold. As the voltage kicking goes on, majority of neurons become more and more closed to the threshold. Thus, whenever a neuron fires, those that are closest to the threshold will also be push to fire. Then the rests will also be pushed by the previous firing events, so on and so forth, just like a threshold crossing avalanche that firing triggers the fire of the other neurons in the short time period.

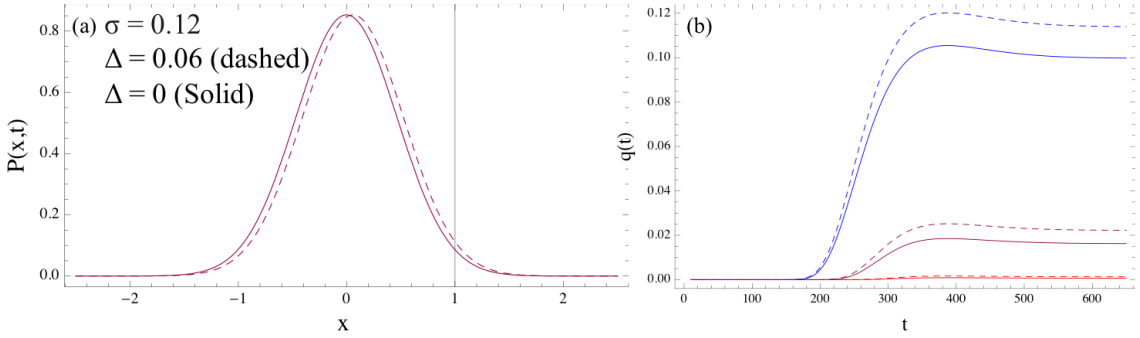

Fig. 5 (a) shows the probability $P(x, t)$ (solid), and $P(x - \Delta, t)$ (dashed) of a single neuron j ,before and after a neuron i's firing ($i \neq j$). (b) the corresponding $q(t)$ before and after the shift of Δ, with different noise level.

IV. Appendix: Solving Probability Density

The probability density $P(x,y,t)$ for the solution of the unconstrained stochastic differential equation[4],

$$P(x,y,t)\Delta x\Delta y = Prob\big(x \le x_j < x+\Delta x, y \le y_j < y+\Delta y\big)\,, at\ time\ t,$$

is a Gaussian, and can be determined by solving the associated Fokker-Plank Equation:

$$\frac{\partial P}{\partial t} = -\frac{\partial}{\partial x}(Ax+By)P - \frac{\partial}{\partial y}(Cx+Dy)P + \frac{\sigma^2}{2}\frac{\partial^2 P}{\partial x^2}\,, \qquad (A.1)$$

which includes four drift terms, and the only one diffusion term owing to the noise input in the x equation. The initial conditions at an initial time t_0 are given by

$$P(x,y,t_0) = \delta\big(x-x(t_0)\big)\delta\big(y-y(t_0)\big). \qquad (A.2)$$

Here, we are interested in the evolution of $P(x,y,t)$ just after an action potential generates, so we take initial conditions at $t_0 = 0$ as the reset times t_0 following an action potential, and set $x(t_0) = x_{reset}$ and $y(t_0) = y + y_{reset}$ as well. If we express $P(x,y,t)$ by its Fourier trans-form with respect to x and y, i.e., by

$$P(x,y,t) = \frac{1}{(2\pi)^2}\int dk_1 \int dk_2 e^{i(k_1x+k_2y)}\hat{P}(k_1,k_2,t)\,, \qquad (A.3)$$

we obtain the Fourier transform of Eq.(??) by replacing $\partial_{x,y}$ with $ik_{1,2}$ and x (or y) with $i\partial_{k_1}$ (or $i\partial_{k_2}$),

$$\begin{aligned}\frac{\partial \hat{P}}{\partial t} &= (Ak_1+Ck_2)\frac{\partial \hat{P}}{\partial k_1} + (Bk_1+Dk_2)\frac{\partial \hat{P}}{\partial k_2} - \frac{\sigma^2}{2}k_1^2\hat{P} \\ &= -\gamma_{ij}k_i\frac{\partial \hat{P}}{\partial k_j} - d_{ij}k_ik_j\hat{P}\,, \qquad (A.4)\\ \gamma_{ij} &= -\begin{pmatrix} A & B \\ C & D\end{pmatrix}, \qquad d_{ij} = \begin{pmatrix}\sigma^2/2 & 0 \\ 0 & 0\end{pmatrix},\end{aligned}$$

with initial condition $\hat{P}(k_1,k_2,t) = \exp(-i(k_1x_0+k_2y_0))$. Since we already know that P is a Gaussian and therefore make the 'ansatz' that $\hat{P}$ is a Gaussian as well, and the solution is

$$\hat{P}(k_1,k_2,t) = \exp\left(-iM_i(t-t_0) - \frac{1}{2}k_ik_jN_{ij}(t-t_0)\right)$$

where $M_i(t)$ and $N_{ij}(t)$ $(i,j = 1,2\,)$ are moments and variances. Insert this 'ansatz' in to Eq. (A.4) and get

$$\frac{\partial \hat{P}}{\partial t} + \gamma_{ij}k_i\frac{\partial \hat{P}}{\partial k_j} + d_{ij}k_ik_j\hat{P} = \left(-ik_i\dot{M}_i - \frac{1}{2}k_ik_j\dot{N}_{ij} - \gamma_{ij}k_iN_{jl}k_l - i\gamma_{ij}k_iM_j + d_{ij}k_ik_j\right)\hat{P} = 0,$$

the equation requires that M_j and N_{lj} must satisfy the following ODEs

$$\dot{M}_i = -\gamma_{ij}M_j, \qquad \dot{N}_{ij} = -\gamma_{ij}N_{jl} - \gamma_{jl}N_{li} + 2d_{ij}.$$

And then we follow the approaches shown in (Risken, 1989), calculated $M_{1,2}$ and N_{ij} with Mathematica, and eventually we get

$$\begin{aligned}N_{11} &= \frac{\sigma^2}{2(\lambda_2-\lambda_1)^2}\left\{\frac{(\lambda_1+\mathrm{D})^2\big(1-e^{-2t\lambda 1}\big)}{\lambda_1} + \frac{(\lambda_2+\mathrm{D})^2(1-e^{2t\lambda 2})}{\lambda_2} - \frac{4BC(e^{-t(\lambda_1+\lambda_2)}-1)}{\lambda_1+\lambda_2}\right\}\\ N_{12} &= \frac{C\sigma^2}{2(\lambda_2-\lambda_1)^2}\left\{\frac{-(\lambda_1+\mathrm{D})\big(1-e^{-2t\lambda 1}\big)}{\lambda_1} - \frac{(\lambda_2+\mathrm{D})(1-e^{2t\lambda 2})}{\lambda_2} + \frac{2(a-d)(-1+e^{-t(\lambda 1+\lambda 2)})}{\lambda_1+\lambda_2}\right\}\end{aligned}$$

[4] The x can be larger than the threshold x_{thres} because FPE is not involved in the resetting mechanism of x and y, which is applied when simulating the two SDEs Eq. (3) and (4).

$$N_{22} = \frac{c^2\sigma^2 e^{-3t(\lambda 1+\lambda 2)}\left\{e^{3t(\lambda 1+\lambda 2)}(\lambda_2-\lambda_1)^2 + 4e^{2t(\lambda 1+\lambda 2)}\lambda_1\lambda_2 - \left(e^{t(3\lambda 1+\lambda 2)}\lambda_1 + e^{t(\lambda 1+3\lambda 2)}\lambda_2\right)(\lambda_1+\lambda_2)\right\}}{2\lambda_1\lambda_2(\lambda_2-\lambda_1)^2(\lambda_1+\lambda_2)}$$

where $\lambda_{1,2}$ is the eigenvalue of matrix γ

$$\lambda_{1,2} = \frac{-(A+D) \mp \sqrt{(A-D)^2+4BC}}{2}$$

The probability density is

$$P(x,y,t) = \frac{1}{2\pi\sqrt{N_{11}N_{22}-N_{12}^2}} \exp\left\{-\frac{1}{2\left(1-\frac{N_{12}^2}{N_{11}N_{22}}\right)}\left(\frac{(x-M_1)^2}{N_{11}} - \frac{2N_{12}(x-M_1)(y-M_2)}{N_{11}N_{22}} + \frac{(y-M_2)^2}{N_{22}}\right)\right\}.$$

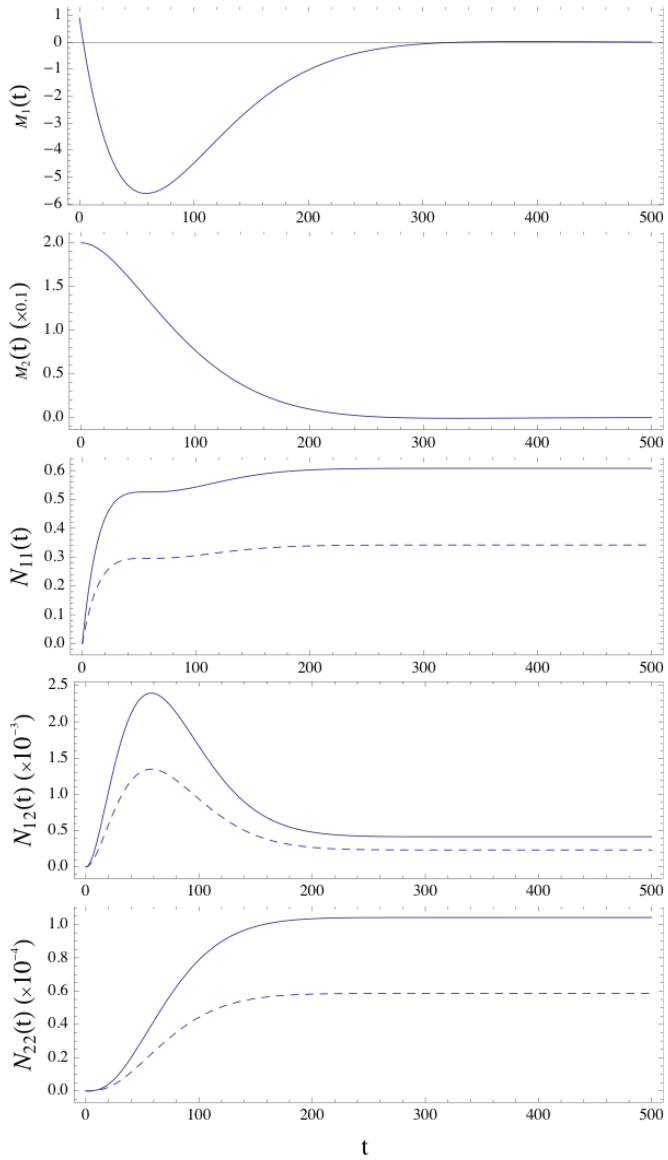

Fig. A1 The plot of $M_{1,2}(t)$, $N_{11}(t)$, $N_{12}(t)$ and $N_{22}(t)$.

V. Reference

1. B Lindner et al., Noise effect in the excitable system, Phys. Reports 392, 321–424 (2004).
2. S. Reinker et al., Noise-Induced Coherence and Network Oscillations in a Reduced Bursting Model, Bulletin of Math. Biology 68:6, 1401-1427 (2006).

3. S. Reinker et al., Resonances and Noise in a Stochastic Hindmarsh–Rose Model of Thalamic Neurons, Bulletin of Math. Biology 65, 641–663 (2003).
4. J. M. Buldú et al., Effect of external noise correlation in optical coherence resonance, Phys. Rev. E 64, 051109 (2001)
5. G. Giacomelli, Phys. Rev. Lett. 84, 3298 (2000).
6. I. Fischer, Phys. Rev. Lett. 76, 220 (1996).
7. R. Lang, K. Kobayashi, IEEE J. Quantum Electron. QE-16, 347 (1980).
8. G.H.M. van Tartwijk, G.P. Agrawal, Prog. Quantum Electron. 22, 43-122 (1998).
9. J. Mulet and C. R. Mirasso, Phys. Rev. E 59, 5400 (1999).
10. C.H. Henry, R.F. Kazarinov, IEEE J. Quantum Electron. QE-22, 294 (1986).
11. G.H.M. van Tartwijk, D. Lenstra, Quantum Semiclass. Opt. 7, 87 (1995).